Journal of Transport Geography 131 (2026) 104541

Contents lists available at ScienceDirect

Journal of Transport Geography

journal homepage: www.elsevier.com/locate/jtrangeo

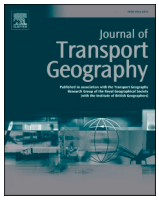

Evaluating human mortality impacts from air pollution as U.S. commuting reaches its extremes

Yue Jing [a,c], Yujie Hu [a,*], Chen Chen [b], Daniel S. Cohan [b]

[a] Department of Geography, University of Florida, Gainesville, FL 32611, USA
[b] Department of Civil and Environmental Engineering, Rice University, Houston, TX 77005, USA
[c] Department of Geography & Geographic Information Science, University of North Dakota, Grand Forks, ND 58202, USA

ARTICLE INFO

Keywords:
Excess commuting
Urban form
Emission
Air pollution
Mortality
Human mobility
Spatial networks

ABSTRACT

Commuting significantly influences environmental quality and public health, thereby shaping urban sustainability. However, the effects of air pollution from vehicle emissions and associated mortality at both lower and upper commuting extremes remain unexplored. This study utilizes nationwide commuting flow and geodemographic segmentation datasets to implement a disaggregated excess commuting framework across 918 U.S. metropolitan regions (MSAs). Three reduced-complexity air quality health effect models are then employed to assess changes in vehicle emissions and related mortality for these extreme scenarios. Results show that achieving the minimum commuting scenario could prevent approximately 1273 premature deaths nationwide, whereas the maximum commuting scenario could result in 3480 additional deaths linked to elevated air pollution. These impacts vary considerably across urban forms and regions, with densely populated, polycentric MSAs accounting for over 70 % of total mortality changes. In some MSAs, health outcomes diverge from emission changes due to geographic factors that influence pollutant dispersion. Overall, the findings highlight the need for targeted policies that promote more sustainable and health-conscious mobility systems.

1. Introduction

The adverse effects of air pollution, including nitrogen oxides (NO_x = NO and NO_2), volatile organic compounds (VOCs), and particulate matter (PM), on human health have become a global sustainability concern. In 2021, air pollution accounted for 8.1 million deaths globally (Health Effects Institute, 2024). Notably, in the United States, the transportation sector is a key contributor to air pollution, accounting for approximately 45 % of NO_x emissions and a substantial share of VOC and PM emissions (U.S. Environmental Protection Agency, 2020). Reducing emissions from transportation, especially from work-related commuting that drives two daily traffic peaks, has therefore been a persistent challenge for policymakers.

Extensive research highlights the effectiveness of planning initiatives in influencing travel behavior (Boarnet and Crane, 2001; Boarnet, 2011; Bruns and Matthes, 2019). One widely used strategy to reduce commuting and related air pollution is promoting jobs-housing balance, which seeks to bring residential areas and workplaces closer together (Cervero, 1989). Through targeted planning and initiatives (Baltimore City Department of Housing and Community Development, 2021; District of Columbia Office of Planning, 2011), workers can be incentivized to relocate homes or change jobs without changing existing land use. This approach has the potential to reduce a region's commuting distances to the lowest possible level associated with an optimal jobs-housing balance, enabling residents, on average, to work at locations nearest to their homes. However, this scenario represents only the *lower commuting extreme* a region can achieve. In the absence of effective planning and management, a region may also reach the *upper commuting extreme*, characterized by maximized commuting distances resulting from the most imbalanced jobs-housing relationship, where residents, on average, work at locations farthest from their homes.

The lower and upper commuting extremes correspond to, respectively, the minimum and maximum commuting scenarios a region can achieve without altering existing land use. These extremes, calculated based on the spatial distribution of jobs and residences, provide a measure of jobs-housing proximity and are widely used as indicators for evaluating urban form (Chowdhury et al., 2013; Ha et al., 2021). The difference between the region's actual commuting distance and the minimum commute, as well as the commuting capacity defined by the gap between the maximum and minimum commutes, reflects the

* Corresponding author.
E-mail address: yujiehu@ufl.edu (Y. Hu).

https://doi.org/10.1016/j.jtrangeo.2025.104541
Received 26 August 2025; Received in revised form 11 November 2025; Accepted 21 December 2025
Available online 24 December 2025

region's commuting efficiency and indicates the extent of excess commuting (Hamilton and Röell, 1982), a concept rooted in urban economics.

Over the years, the excess commuting (EC) concept has developed into a widely recognized methodological framework (Horner, 2002; Charron, 2007; Murphy and Killen, 2011; Hu and Wang, 2016; Hu and Li, 2021; Jing and Hu, 2024), playing a pivotal role in shaping transportation and land-use policies aimed at reducing commuting distances and addressing related social and environmental sustainability challenges (Korsu and Le Néchet, 2017; Xu et al., 2019; Yang, 2008). While numerous studies have explored socio-demographic disparities in EC across cities and regions globally (Buliung and Kanaroglou, 2002; Horner and Schleith, 2012; Kim and Horner, 2021; Yue et al., 2024), only three have specifically assessed its environmental impacts (Loo and Chow, 2011; Scott et al., 1997; Welch and Mishra, 2014). However, the changes in emissions and related human health outcomes when a region's commuting reaches its lower or upper extremes remain unexplored. By revealing potential reductions or increases in harmful emissions, this analysis can inform policy interventions aimed at minimizing health risks associated with commuting, ultimately contributing to the development of sustainability-focused benchmarks.

This study aims to evaluate the two commuting extremes—the minimum and maximum commutes that a region's current urban structure can support—and to quantify the potential shifts in air pollutant levels and associated mortality as a region's commuting patterns approach these extremes. This comprehensive analysis encompasses all 918 Metropolitan and Micropolitan Statistical Areas (MSAs) throughout the contiguous United States. This research stands out for several reasons. Primarily, it represents the first effort to explore the environmental and health impacts linked to a region's commuting extremes. Furthermore, it introduces a refined methodology for assessing both minimum and maximum commutes by addressing the prevalent assumption of homogeneity among homes and/or jobs (Frost et al., 1998; Ha et al., 2021; Ma and Banister, 2006; Zhou et al., 2020). Lastly, it is the first nationwide analysis within this scope, offering a more comprehensive and generalized understanding of the environmental and health impacts of commuting extremes. These insights have important implications for developing benchmark metrics for assessing urban sustainability.

2. Literature review

2.1. The excess commuting framework

Initially referred to as wasteful commuting, excess commuting (C_{ex}) quantifies the disparity between the average observed commute (C_{obs}) and optimal (minimum or required) commute (C_{min}) that a city could achieve without altering its land-use configuration. This concept was proposed by Hamilton and Röell (1982) as an assessment of the validity of the traditional monocentric model in predicting actual commuting patterns (Eq. 1). Departing from Hamilton and Röell's approach under the assumption of monocentricity, (White, 1988) employing the LP (Linear Programming) method to calculate C_{min} based on the actual spatial configuration of jobs and housing. This method has since become the prevailing approach in excess commuting studies (Jing and Hu, 2024; Ma and Banister, 2006). Essentially, the LP approach calculates C_{min} by reassigning existing jobs (or housing) to their nearest housing (or jobs), on average, within the current urban configuration. In other words, it redistributes commuting flows between workplaces and residences to minimize the overall commuting cost in the city. Consequently, C_{ex} serves as a metric for evaluating the commuting efficiency of a city, quantifying the city's capacity to minimize its commutes to the utmost extent possible. A higher C_{ex} value suggests a greater surplus of commutes and a less efficient commuting system. The LP method can be formulated as follows (Eqs. 2–3):

$$C_{ex} = \frac{C_{obs} - C_{min}}{C_{obs}} \times 100 \tag{1}$$

$$C_{min} = min\left(\frac{1}{N}\sum_i\sum_j D_{ij}X_{ij}\right) \tag{2}$$

$$\text{Subject to}: \sum_j X_{ij} = W_i, \sum_i X_{ij} = E_j, X_{ij} \geq 0 \tag{3}$$

where X_{ij} is the number of resident workers commuting from zone i to zone j, D_{ij} is the travel distance or time between zones i and j, W_i denotes the total number of resident workers living in zone i, E_j refers to the total number of jobs in zone j, and N is the total number of resident workers in the city.

The original excess commuting concept has been expanded through various extensions, transforming it into a methodological framework focused on commuting efficiency (Charron, 2007; Horner, 2002). One noteworthy effort is the development of the theoretical maximum commute (C_{max}) (Horner, 2002). As formulated in Eqs. 4–6, C_{max} can be calculated following the similar approach to C_{min}, but with an opposing objective function. The difference between the upper and lower commuting bounds (i.e., C_{max} - C_{min}) represents the commuting capacity of a city.

$$C_{max} = max\left(\frac{1}{N}\sum_i\sum_j D_{ij}X_{ij}\right) \tag{4}$$

$$\text{Subject to}: \sum_j X_{ij} = W_i, \sum_i X_{ij} = E_j, X_{ij} \geq 0 \tag{5}$$

In essence, the excess commuting framework consists of two components: metrics related to commuting benchmarks (e.g., C_{min}, C_{obs}, and C_{max}) and metrics that reflect the associated commuting efficiency. These efficiency metrics are derived by comparing the observed commute to various commuting benchmarks. Commuting benchmarks are determined by the spatial relationship between residences and workplaces, shedding light on different aspects of urban form. Specifically, C_{min} represents the minimum required commute for a city given its exiting urban form, indicating the overall spatial proximity between residences and workplaces. A smaller C_{min} signifies a more balanced jobs-housing relationship. In contrast, C_{max} depicts the worst commuting scenario a city might face under the current spatial arrangement of residences and workplaces. It is known to scale with city size and is often used as an indicator of jobs-housing separation and decentralization (Kanaroglou et al., 2015).

2.2. Excess commuting and urban form

The various commuting benchmarks have been widely employed to understand the urban form dynamics, especially in comparative studies spanning diverse geographic regions or time periods. A recent example is the study by Schleith et al. (2019), which aimed to characterize urban form in the United States. Using a hierarchical clustering approach, the study classified 53 largest Metropolitan Statistical Areas in the United States into distinct categories of urban forms, such as polycentric, sprawling, and monocentric, based on a suite of excess commuting metrics. Additionally, some studies integrated the excess commuting framework into Brotchie's urban triangle (Brotchie, 1984)—a classic conceptual model illustrating the relationship between land-use dispersal and commuting length—to explore the dynamics of urban form and commuting efficiency in selected cities over time (Chowdhury et al., 2013; Ha et al., 2021; Ma and Banister, 2007).

2.3. Urban form and commuting-related emissions

Existing studies have acknowledged the connection between urban form and commuting-related environmental impacts. The discussions were grounded in the complex connections between land-use and transportation systems (Loo and Chow, 2011). This body of literature primarily seeks to examine how various urban form indicators, such as density, land use mix, compactness, as well as regional-level characteristics like city size, sprawl, monocentricity, and polycentricity, influence commuting outcomes (e.g., commuting distance/time, mode choice) and associated emissions (Aguiléra and Voisin, 2014; Bereitschaft and Debbage, 2013; Blaudin de Thé et al., 2021; Cervero, 1989; Lee, 2020; Muñiz and Rojas, 2019; Zhang et al., 2024). The conclusions on the relationships between urban form and commuting-related emissions may differ due to variations in geographical contexts, definitions of measurements, and calculation methods. However, empirical evidence from the United States, Europe, and China indicates that higher density, mixed land use, and compactness generally lead to shorter commuting distances, reduced automobile usage, and lower commuting-related emissions by concentrating residences, employment, and other functions (Blaudin de Thé et al., 2021; Cervero, 1989). At the regional level, discussions often revolve around the environmental performance of various urban forms, such as monocentric, polycentric, and sprawling forms. Polycentricity is often advocated as a design strategy to mitigate commuting-related emissions because multiple sub-centers can attract commuting flows from primary centers, thereby reducing congestion and promoting the use of mass transit options (Muñiz and Garcia-López, 2019; Sultana, 2002; Susilo and Maat, 2007). However, conflicting evidence suggests that compared to monocentric forms, polycentric cities may entail longer commuting distances/times, potentially leading to increased emissions, due to the dispersion of employment opportunities (Burgalassi and Luzzati, 2015; Hu and Wang, 2016; Schwanen et al., 2004).

3. Methods

3.1. Study area and data sources

This nationwide study encompasses 918 MSAs across the contiguous United States. Three major sources of datasets are utilized in this study. 1) Neighborhood data: to obtain a more accurate estimation of EC, this study relaxes the homogeneity assumption among workers and disaggregates resident workers into distinct subgroups according to their residential neighborhood types. The neighborhood type data are obtained from the 2020 Esri Tapestry Segmentation (*Esri* Tapestry Segmentation—Esri Demographics Regional Data | Documentation, 2020), which classifies census tracts in the United States into 14 types of distinct life modes based on a combination of socioeconomic, housing,

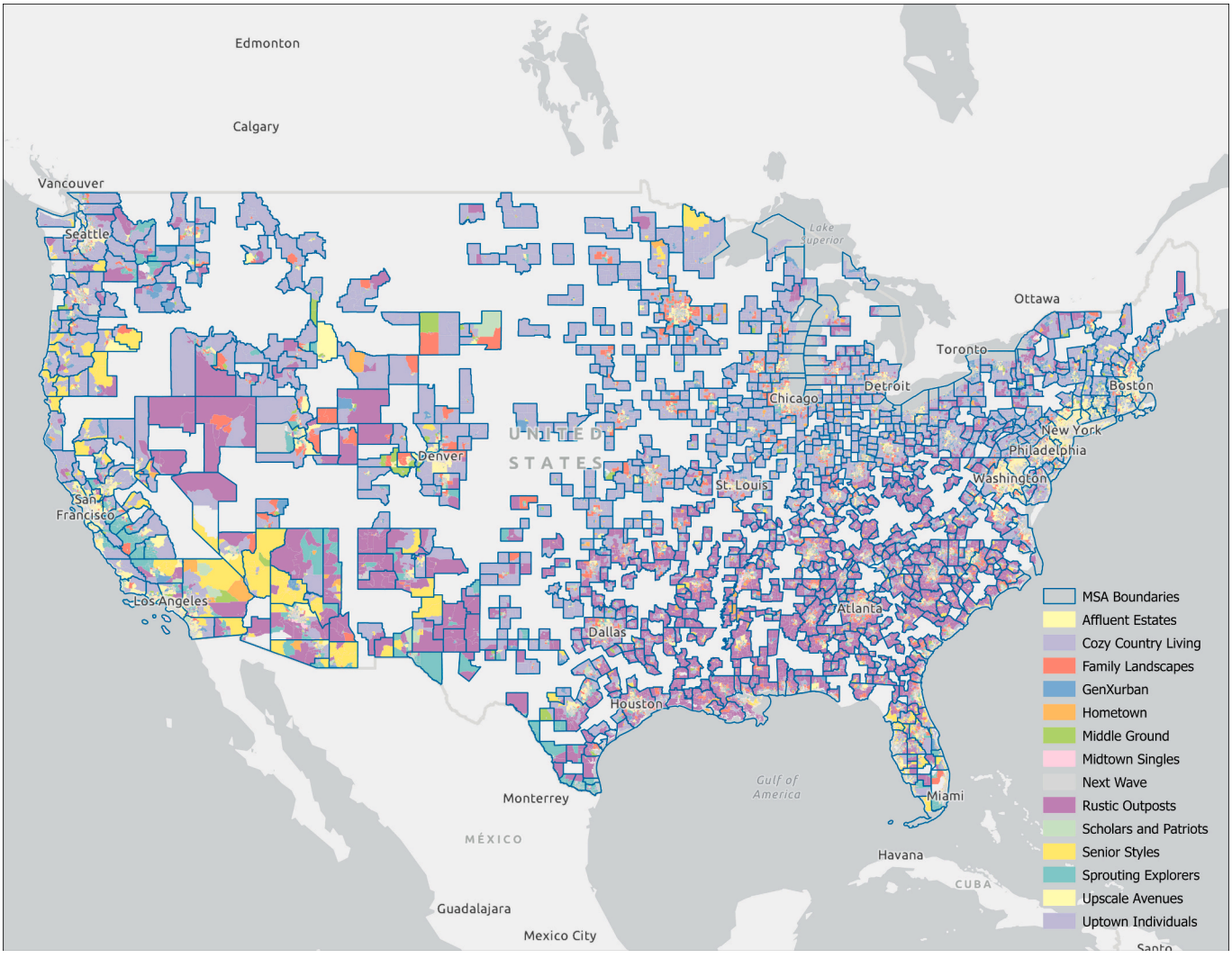

Fig. 1. Spatial distribution of the 14 life modes across MSAs. [Note: A detailed explanation of the classification methodology and descriptions of the 14 lifestyle segments can be found in the accompanying Esri documentation (*Esri* Tapestry Segmentation—Esri Demographics Regional Data | Documentation, 2020).]

and lifestyle attributes. (see Fig. 1). 2) Commuting flow data: the observed commuting flows come from the origin-destination (O—D) pairs of the 2018 LEHD Origin-Destination Employment Statistics dataset provided by the U.S. Census Bureau. This dataset contains the number of commuters between census blocks across the United States. For consistency, this study aggregates the block-level commuting flows at the tract level. 3) Geographic data: the 2018 geographic boundaries and road network data are obtained from the U.S. Census Bureau. The location of CBD (Central Business District) centers or central landmarks for each MSA is collected using the geocoding API provided by Google Maps.

3.2. Assessing commuting extremes through a disaggregated EC framework

To address the strict homogeneity assumption among workers, this study introduces a disaggregated EC analysis based on the widely used LP approach. It calculates three key commuting benchmarks—observed distance (C_{obs}), minimum distance (C_{min}), and maximum distance (C_{max})—along with two corresponding EC metrics, C_{ex} and C_u, across 14 distinct neighborhood types within the 918 MSAs in the United States. As demonstrated in Eq. 6, for neighborhood group k within a given MSA, C_{ex}^k compares C_{obs}^k with C_{min}^k to assess how much the actual commuting distances of resident workers in those neighborhoods exceed their group's minimum level. A higher C_{ex}^k value indicates a greater surplus of commuting, reflecting a less efficient commuting pattern for that group. C_u^k, on the other hand, further includes C_{max}^k in the comparison to evaluate how much of group k's available commuting capacity (the gap between C_{min}^k and C_{max}^k) is already utilized (see Eq. 7). A higher C_u^k value suggests a stronger tendency toward the upper commuting limit C_{max}^k, indicating lower commuting efficiency for that group.

$$C_{ex}^k = \frac{C_{obs}^k - C_{min}^k}{C_{obs}^k} \times 100 \tag{6}$$

$$C_u^k = \frac{C_{obs}^k - C_{min}^k}{C_{max}^k - C_{min}^k} \times 100 \tag{7}$$

To calculate C_{min}^k and C_{max}^k, the LP approach is applied to each neighborhood type k within each MSA. The goal of introducing neighborhood-type disaggregation is to better capture the heterogeneity among workers that is often overlooked in traditional EC frameworks. The original approach assumes all workers are homogeneous and can freely exchange their residences or jobs, which can bias the estimation of commuting extremes. In essence, the LP approach determines C_{min}^k (or C_{max}^k) by reallocating existing jobs (or housing) of group k to the overall nearest (or farthest) available housing (or jobs) within that group. Compared to the traditional method that assumes uniformity in jobs and housing for all resident workers, disaggregating by neighborhood types allows for a more nuanced understanding of the differences in residential and employment patterns among commuters. Hence, this approach improves the accuracy of commuting benchmarks and EC estimates. Eq. 8 provides the formula for calculating C_{min}^k:

$$C_{min}^k = min\left(\frac{1}{N_k}\sum_{i\in k}\sum_{j} D_{ij}X_{ij}\right) \tag{8}$$

Subject to:

$$\sum_j X_{ij} = W_i^k \forall i \in k,$$

$$\sum_k \sum_{i\in k} X_{ij} = E_j$$

$$X_{ij} \geq 0 \tag{9}$$

where X_{ij} is the number of resident workers commuting from tract i to tract j, D_{ij} is the travel distance between tracts i and j, W_i^k denotes the total number of resident workers residing in tract i that is classified as group k, E_j refers to the total number of jobs in tract j, and N_k is the total number of resident workers of group k within the MSA. The overall $\overline{C}_{min}$ for the entire workforce in the MSA is then determined by taking the weighted average of C_{min}^k across all groups, using N_k as the weighting factor (see Eq. 10).

$$\overline{C}_{min} = \frac{\sum_k N_k C_{min}^k}{\sum_k N_k} \tag{10}$$

Similarly, C_{max}^k is computed using the same approach as C_{min}^k, but with the opposing objective function (refer to Eqs. 11 and 12), and the overall $\overline{C}_{max}$ for the entire workforce in the MSA is calculated by taking the weighted average of C_{max}^k across all groups, using N_k as the weighting factor (see Eq. 13).

$$C_{max}^k = max\left(\frac{1}{N_k}\sum_{i\in k}\sum_{j\in k} D_{ij}X_{ij}\right) \tag{11}$$

Subject to:

$$\sum_j X_{ij} = W_i^k \forall i \in k,$$

$$\sum_k \sum_{i\in k} X_{ij} = E_j$$

$$X_{ij} \geq 0 \tag{12}$$

$$\overline{C}_{max} = \frac{\sum_k N_k C_{max}^k}{\sum_k N_k} \tag{13}$$

The classification of each census tract into a specific neighborhood type k is based on the 2020 Esri Tapestry Segmentation data (*Esri* Tapestry Segmentation—Esri Demographics Regional Data | Documentation, 2020). The values for W_i^k and E_j for a tract is calculated from the LEHD commuting flow dataset. The commuting cost D_{ij} consists of two main components: interzonal distance and intrazonal distance. The interzonal distance is calculated as the shortest path distance along the road network between the centroids of two tracts. The intrazonal distance, as per Jing et al. (2023), is computed as the radius of a circle that approximates the area of the tract. The total travel distance between two tracts is then determined by adding both interzonal and intrazonal distances, thereby encompassing the additional travel between home or job locations and their respective tract centroids (Hu et al., 2020).

Subsequently, these data are input into Eqs. 8–13 to derive the two commuting benchmarks ($\overline{C}_{min}$ and $\overline{C}_{max}$) for each MSA. The value for C_{obs} for each MSA is obtained based on the observed commuting flow from the LEHD dataset and D_{ij} between two tracts. Finally, EC metrics (C_{ex} and C_u) are computed by comparing C_{min} or C_{max} with C_{obs} for each MSA.

3.3. Classifying MSAs based on land-use variables

The second analysis focuses on categorizing MSAs into various classes of urban form, which is associated with a region's commuting performance. For a more in-depth examination of urban form typologies across the 918 MSAs, this study adopts the approach of Schleith et al. (2019), utilizing a combination of SOM (Self-Organizing Maps) and k-means clustering techniques. This methodology is applied to classify MSAs into distinct urban form classes based on the six land-use variables presented in Table 1. These variables include the number of resident workers (N_w) and the estimated commuting benchmarks, which capture various scenarios of spatial proximity between jobs and housing. In

Table 1
Emission rates for light-duty vehicles in 2018 (version date: 6/8/2021).

	Total HC	Exhaust CO	Exhaust NO_x	Exhaust $PM_{2.5}$	Brakewear $PM_{2.5}$	Tirewear $PM_{2.5}$	CO_2
Raw emission rates (grams/mile)	0.328	4.646	0.256	0.005	0.003	0.001	373.775
	VOC		NO_x		Primary $PM_{2.5}$		
Model inputs (grams/mile)	0.328		0.256		0.009		

particular, C_{min} represents the minimum required commute for a region given its existing urban form, indicating the overall spatial proximity between residences and workplaces. A smaller C_{min} signifies a more balanced jobs-housing relationship. In contrast, C_{max} depicts the worst commuting scenario a region might face under the current spatial arrangement of residences and workplaces. It is often used as an indicator of jobs-housing separation and decentralization. Additionally, this study incorporates concepts from Brotchie's urban triangle model, incorporating jobs-housing dispersal (*DI*) and housing dispersal (C_{CBD}) indices into the classification procedure (Brotchie, 1984). All variables are standardized into z-scores to mitigate the impact of different scales on the classification process.

The classification process involves two primary steps. First, the SOM, also known as Kohonen map, is employed to reveal the underlying structure and relationships of the included variables. The SOM is a special form of an artificial neural network that can map high-dimensional input data onto a two-dimensional space through an unsupervised training algorithm (Arribas-Bel and Schmidt, 2013; Delmelle, 2017). The resulting two-dimensional layer consists of a regular lattice of squares or hexagons known as neurons, each holding a vector corresponding to the multi-dimensional attributes of the input data. Through an iterative process of comparing input observations to output neurons, observations are assigned to neurons based on the shortest Euclidean distances. As a result, observations with shared characteristics will be mapped to nearby regions on the SOM output. Essentially, the MSAs are rearranged in a topological two-dimensional space according to the similarity of the land-use variables. The output of SOM provides crucial insights into the statistical relationship of the multi-dimensional attributes with spatial representation, providing valuable support for the subsequent classification analysis in the next step. Specifically, building on the SOM results, the *k*-means algorithm is then used to partition the two-dimensional topological space into distinct subregions for revealing the inherent urban form typologies of MSAs.

3.4. Examining environmental and health impacts at commuting extremes

The third analysis encompasses the estimation of environmental and health impacts at the two commuting extremes, as derived from the preceding analyses. This involves quantifying alterations in air pollutant levels linked to vehicular traffic resulting from shifts in commuting flows between the observed scenario and the two baseline (minimum and maximum) commuting scenarios. Additionally, the analysis estimates the health effects caused by changes in air pollutant levels resulting from vehicle emissions.

Linking vehicle emissions to health effects implicitly involves three steps – simulating how vehicle emissions affect ambient concentrations of key pollutants, notably ground-level ozone and particulate matter; assessing the populations exposed to those changes in pollutant concentrations; and computing the health effects of those changes in population exposure. Traditionally, completing such analysis has required linking multiple highly complex and computationally intensive models. Specifically, it required meteorological models and emissions models to provide necessary inputs, photochemical models to compute air quality changes resulting from the emissions changes, and health effect models to compute associated impacts on health (Grell et al., 2005; Byun and Schere, 2006; Skamarock et al., 2008; Sacks et al., 2018). Reduced-complexity models simplify the process by assembling results from many runs of the photochemical and health effect models under a variety of meteorological conditions in order to directly link changes in emissions to changes in health outcomes. Here, three reduced-complexity air quality health effect models are utilized: the Estimating Air pollution Social Impact Using Regression (EASIUR) model (Heo et al., 2016), the Air Pollution Emission Experiments and Policy Analysis Version 3 (AP3) model (Muller, 2014), and the Intervention Model for Air Pollution (InMAP) (Tessum et al., 2017).

EASIUR is an online model that directly estimates mortality caused by emissions of $PM_{2.5}$ and its precursors— sulfur dioxide (SO_2), NO_x, and ammonia (NH_3). It utilizes regression analysis on a dataset of small emissions perturbations from 100 sample locations modeled using the CAMx photochemical model (ENVIRON, 2014), with simulations reflecting 2005 conditions. EASIUR reports marginal health damages ($/t) across four seasons and three stack heights. The default concentration-response function (CRF) is sourced from an American Cancer Society (ACS) cohort study (Krewski et al., 2009). Recent studies have shown that these models produce consistent health impact simulations, comparable to three-dimensional air quality models (Chen et al., 2022; Gilmore et al., 2019; Industrial Economics, Inc, 2019).

AP3 is an updated version of the APEEP model, used for air pollution policy analysis in the United States. It models county-level $PM_{2.5}$ and precursor emissions, processing their atmospheric transport, chemical transformation, and deposition across the contiguous United States. This model links emissions from source counties to changes in ambient $PM_{2.5}$ levels in receptor counties through a precomputed source-receptor (S-R) matrix obtained from a modified Gaussian plume model (Chowdhury et al., 2013; Turner, 2020). AP3 estimates health impacts using a CRF that correlates average annual $PM_{2.5}$ concentrations with mortality in adults over 30 and infants under one year (Krewski et al., 2009; Woodruff et al., 2006).

InMAP leverages spatially resolved annual average photochemical relationships from the WRF-Chem meteorological and photochemical model (Grell et al., 2005) to simulate primary and secondary $PM_{2.5}$ formation and transport. InMAP also developed a S-R matrix to create spatially explicit ambient $PM_{2.5}$ concentration differences caused by primary $PM_{2.5}$ emissions and precursor emissions. InMAP operates at a variable spatial resolution, with cell lengths ranging from 1 to 288 km depending on population density, and calculates premature mortalities using an embedded CRF that incorporates relative risks studies (Krewski et al., 2009; Lepeule et al., 2012).

To measure vehicular traffic-related air pollutant levels, the daily one-way commutes reported in the LEHD data are extrapolated to annual two-way commutes. This conversion facilitates the measurement of total changes in commuting distances on a yearly basis under either the minimum or maximum commuting scenarios. The decision for yearly aggregation aligns with the availability of data on vehicular emission rates, sourced from the Bureau of Transportation Statistics.[1] The emission rates are cataloged by calendar year using the U.S. Environmental Protection Agency's Motor Vehicle Emission Simulator (MOVE S3).[2] For consistency with the commuting data, this research utilizes emission rates for the year 2018. The air pollutants considered in

[1] Estimated U.S. Average Vehicle Emissions Rates per Vehicle by Vehicle Type Using Gasoline and Diesel https://www.bts.gov/content/estimated-national-average-vehicle-emissions-rates-vehicle-vehicle-type-using-gasoline-and

[2] MOtor Vehicle Emission Simulator (MOVES): https://www.epa.gov/moves/latest-version-motor-vehicle-emission-simulator-moves (version date: 6/8/2021)

this study include total hydrocarbon (HC), carbon monoxide (CO), nitrogen oxides (NO_x), and primary particulate matter ($PM_{2.5}$), comprising exhaust $PM_{2.5}$, brakewear $PM_{2.5}$, and tirewear $PM_{2.5}$. It is assumed that all changes originate from light-duty vehicles, and only HC (or volatile organic compounds, VOC), NO_x, and primary $PM_{2.5}$ are input into the reduced complexity models. Table 1 presents a comparison between the emission rates from the raw source and the rates used in the study.

Each reduced-complexity model is employed to compute the health impacts of vehicle emissions changes from each MSA. Mortality changes are derived from both the MSA where emissions originate and the neighboring MSAs affected by those emissions. Since the EASIUR model does not estimate mortality from VOC-induced $PM_{2.5}$, VOC-caused mortality estimates are sourced from AP3 and incorporated into the EASIUR results.

To minimize run times in InMAP, which exceeds two hours per run, an initial scenario is executed using emissions from all MSAs. Following this, individual scenarios are conducted for the 20 MSAs with the highest mortality changes. The remaining mortality, representing 22.8 % (19.7 %) of the total reduction (increase), is allocated to the other MSAs based on their mortality change ratios derived from the overall emission reduction scenario in InMAP.

4. Results and discussion

4.1. Commuting extremes across U.S. MSAs

Fig. 2 shows the spatial distribution of positive differences in commuting flows between the minimum (and maximum) and current commuting patterns. Under the minimum scenario, commuting flows generally shift toward shorter distances, with about 80 % of the increase concentrated within 10 miles or less. In contrast, the maximum commuting scenario shows a wider spatial reach, with a higher frequency of cross-commuting flows over longer distances. Notably, approximately 80 % of the increase in commuting flows occurs within the 0–45-mile range. Commuting efficiency varies significantly across MSAs, as reflected by C_{ex} values ranging from 0.64 % to 63.02 %, with an average of 25.2 %. A large portion of MSAs fall within the 15 % to 30 % C_{ex} range. Fig. 3 illustrates that higher C_{ex} values are prominent in densely populated metropolitan regions, especially in the northeastern and western coastal areas, such as Los Angeles, Philadelphia, Houston, and New York. In these areas, C_{ex} exceeds 50 %, indicating substantial potential for reducing commuting burden and improving commuting efficiency. Table 2 presents the top 20 MSAs with the highest C_{ex} values, with Los Angeles and Miami topping the list, each surpassing 60 % in EC.

4.2. Urban form typologies of U.S. MSAs

The output of the SOM algorithm is presented in Fig. 4a, illustrating the organization of MSAs in the topological space based on their similarities across six selected land-use variables. These variables are chosen partially with reference to Brotchie's urban triangle (Brotchie, 1984). Additional details on these variables can be found in Table 3. In each subplot of Fig. 4a, the color of the neuron corresponds to the standardized value associated with that specific variable. Clearly, the distribution of N_w stands out as notably different from the other five variables, displaying a more polarized pattern. MSAs with the highest number of workers predominantly cluster at the upper-left corner, creating a distinct contrast with other regions. In contrast, the remaining variables exhibit a gradient pattern, showing a smooth transition from higher to lower values. Specifically, for C_{min} and C_{obs}, neurons situated in the right upper corner generally have higher values, gradually decreasing downward. Similarly, the outputs of C_{max} and C_{CBD} follow a

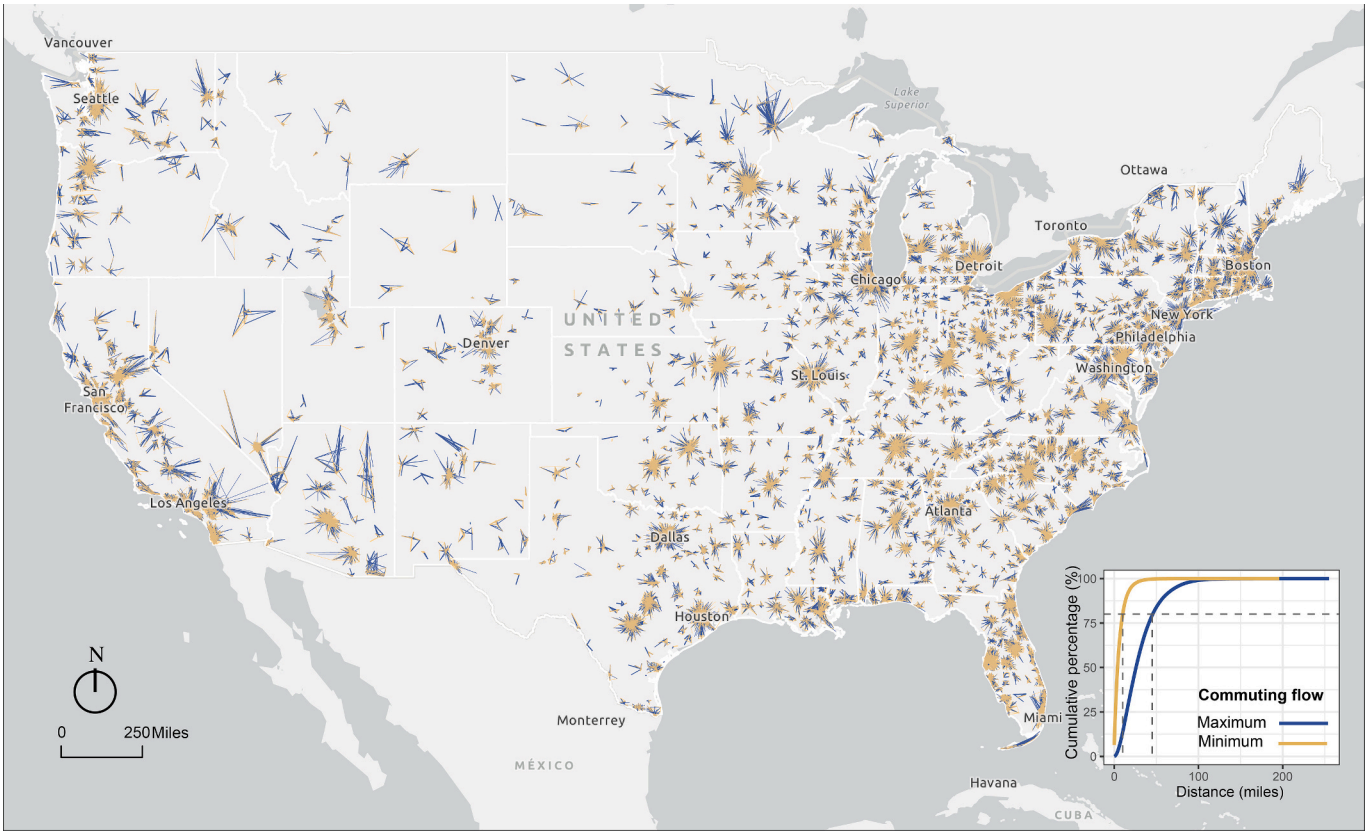

Fig. 2. Spatial distribution of the positive differences between minimum (maximum) and actual commuting flows. [Note: To highlight areas where flows are being reallocated, the map only shows links with differences greater than zero. For each MSA, the top 80 % of flows by cumulative percentage are displayed for visualization purposes.]

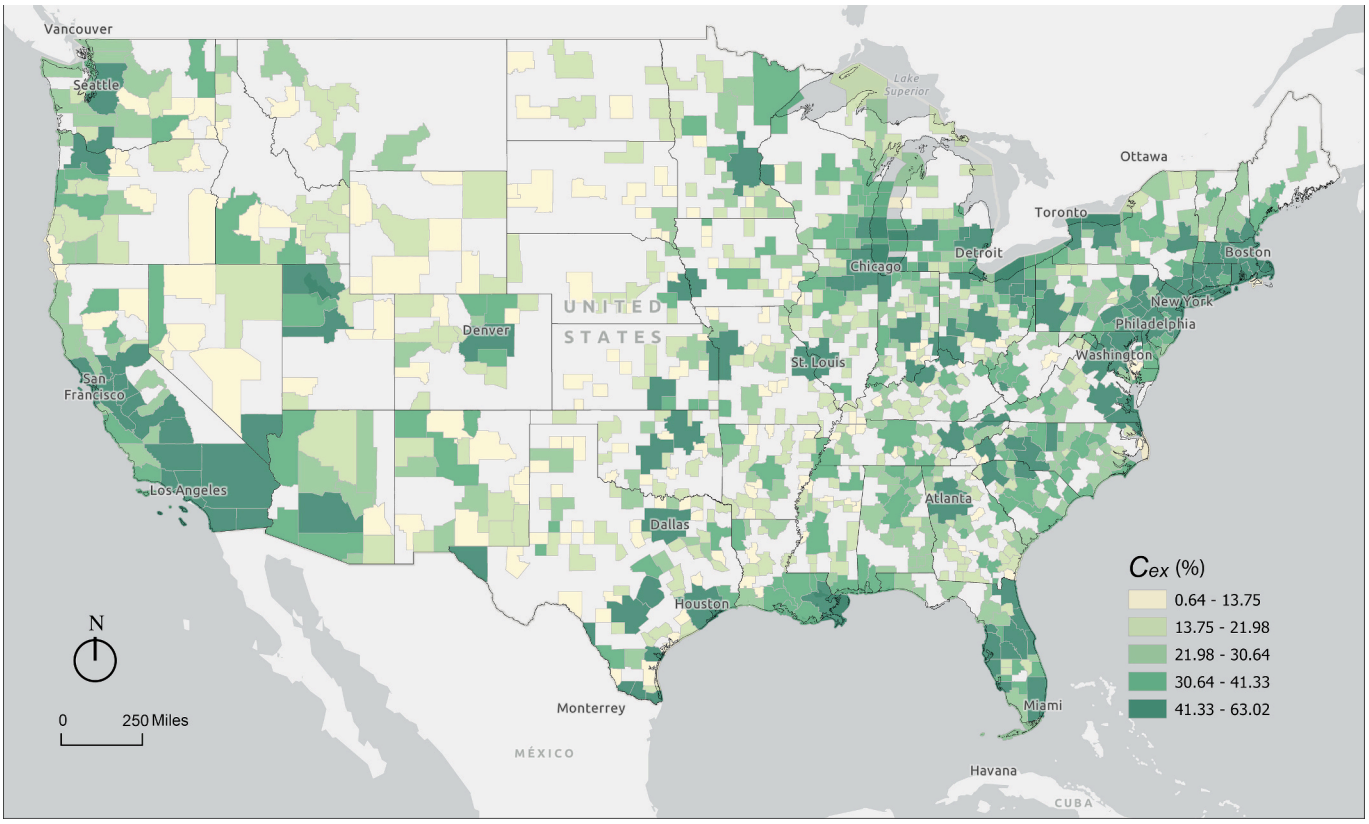

Fig. 3. Spatial distribution of C_{ex} values.

Table 2
Top 20 MSAs with the highest C_{ex} values.

Rank	MSA	C_{ex} (%)	Rank	MSA	C_{ex} (%)
1	Los Angeles-Long Beach-Anaheim, CA	63.02	11	McAllen-Edinburg-Mission, TX	54.19
2	Miami-Fort Lauderdale-Pompano Beach, FL	60.16	12	Brownsville-Harlingen, TX	53.87
3	Riverside-San Bernardino-Ontario, CA	57.05	13	Dallas-Fort Worth-Arlington, TX	53.30
4	Providence-Warwick, RI-MA	56.77	14	Scranton-Wilkes-Barre, PA	53.08
5	Palm Bay-Melbourne-Titusville, FL	56.13	15	Baltimore-Columbia-Towson, MD	52.92
6	Philadelphia-Camden-Wilmington, PA-NJ-DE-MD	55.74	16	San Francisco-Oakland-Berkeley, CA	52.85
7	Virginia Beach-Norfolk-Newport News, VA-NC	55.27	17	New York-Newark-Jersey City, NY-NJ-PA	52.78
8	Pittsburgh, PA	55.02	18	Youngstown-Warren-Boardman, OH-PA	52.46
9	Detroit-Warren-Dearborn, MI	54.94	19	New Haven-Milford, CT	51.95
10	Houston-The Woodlands-Sugar Land, TX	54.33	20	Dayton-Kettering, OH	51.38

comparable pattern with a smooth decrease from top to bottom. This outcome suggests a notable correlation between C_{max} and C_{CBD}, in line with existing studies (Kanaroglou et al., 2015). In contrast, *DI* presents a distinct pattern, with MSAs having the highest degree of jobs-housing dispersion concentrated at the bottom-left corner.

Building upon the initial arrangement of MSAs on the SOM output map, the *k*-means clustering algorithm is then employed to partition the two-dimensional topological space into cohesive sub-regions based on the weight vector of each neuron corresponding to the six land-use variables. As shown in Fig. 4b, the 918 MSAs are classified into five distinct categories, each depicted as a non-overlapping sub-region in SOM output space. Importantly, the proximity between any two categories indicates the degree of similarity in urban form, as they are arranged based on similarities across the six land-use variables. The urban form characteristics of the five MSA categories are identified through an examination of the mean z-score for each of the land-use variables (see Table 4).

Fig. 4b illustrates three prominent urban form patterns observed in non-adjacent sub-regions of the SOM map—specifically, the upper-left, upper-right, and lower-right corners. The remaining two categories, positioned between the three sub-regions, exhibit a mixture of characteristics from various urban form patterns. Fig. 4c employs Brotchie's urban triangle to depict the relationship between urban from and commuting patterns across the five urban form categories. The shapes of the corresponding triangles reveal the key characteristics of these categories. The spatial distribution of these five categories across the United States is presented in Fig. 5. A description of the profiles associated with these categories is presented below.

Polycentric. This category, located in the upper-left corner of the SOM map, identifies the 15 largest and densely populated polycentric MSAs in United States, including New York, Los Angeles, Chicago, Dallas, Houston, Washington, Philadelphia, Atlanta, Miami, Boston, Phoenix, Minneapolis, San Francisco, Seattle, and Detroit. As shown in the urban triangle, this category exhibits the largest commuting range (C_{max} - C_{min}), indicating greater commuting flexibility. MSAs in this category have high-density development and an overall balanced jobs-housing spatial relationship, facilitated by the presence of multiple

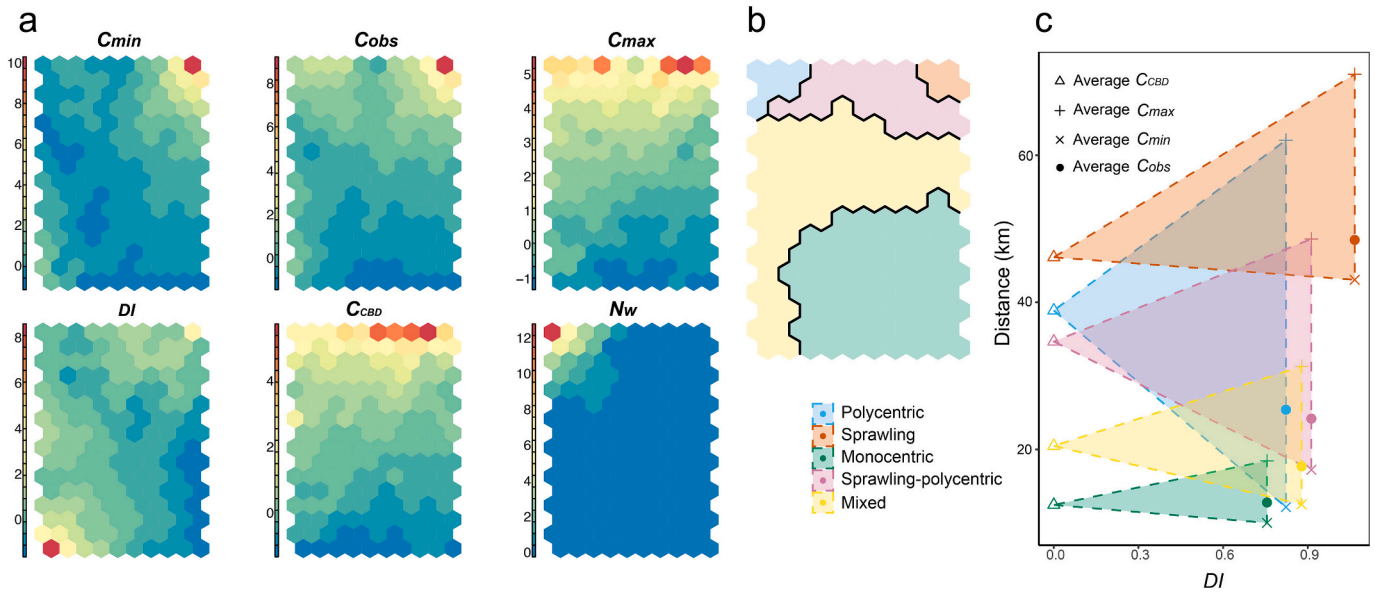

Fig. 4. a, Arrangement of the six land-use variables in SOM output space; b, partition of SOM output space; and c, modified Brotchie's urban triangle.

Table 3
List of the selected land-use variables for the classification of MSAs.

Variables	Descriptions
N_w	Total number of resident workers in a census tract within an MSA
C_{min}	Average minimum commute between census tracts within an MSA
C_{obs}	Average observed commute between census tracts within an MSA
C_{max}	Average maximum commute between census tracts within an MSA
C_{CBD}	A metric of housing dispersal, which is computed as the average distance from workers' residences to the CBD. It serves as an indicator of the spatial extent of the area (Kanaroglou et al., 2015).
DI	A metric of jobs-housing dispersal, which is computed as the ratio of the average distance of jobs from the CBD (jobs dispersal) to the average distance of workers' residences from the CBD (housing dispersal). It ranges from 0 to 1, with 0 indicating a monocentric city and 1 signifying a city where activities are uniformly distributed (Chowdhury et al., 2013).

spatially proximate job and residential clusters. Regarding commuting efficiency, these MSAs have the second-largest C_{obs} and the largest C_{ex}, reflecting significant cross-commuting and lower commuting efficiency. However, the C_u value indicates better utilization of commuting capacity, as the polycentric layout supports a much higher upper limit in commuting.

Sprawling. This category, situated in the upper-right corner of the SOM map, includes 12 of the most sprawling, low-density MSAs, primarily in the Mountain States region. While these areas share some traits with the polycentric group, such as expansive geography and larger C_{max}, they are distinguished by a much higher degree of jobs-housing dispersion and a larger C_{min}, signaling a highly imbalanced spatial relationship between homes and jobs. This imbalance constrains workers' ability to optimize commutes, leading to the highest C_{obs}. Despite the smallest C_{ex} due to the small gap between C_{obs} and C_{min}, this seemingly efficient pattern does not reflect an ideal commuting scenario.

Monocentric. This category, positioned in the lower-right corner of the SOM map, represents the most prevalent urban form, comprising over 50 % of U.S. MSAs, mainly in the Eastern and Central regions, such as El Paso, TX; Colorado Springs, CO; McAllen, TX; Reno, NV; and Lexington, KY. Unlike polycentric and sprawling categories, monocentric MSAs exhibit a more compact development pattern, with the smallest values for *DI*, C_{CBD}, C_{min}, C_{obs}, and C_{max}. They also have the second smallest C_{ex}, indicating a relatively efficient commuting system.

Table 4
Mean z-scores for the land-use and commuting performance variables across five MSA categories.

	C_{min}	C_{obs}	C_{max}	*DI*	C_{CBD}	N_w	C_{ex}	C_u	Percentage of MSAs (%)	Representative MSAs (Top 5 ranked by N_w)
Polycentric	0.04	1.53	2.65	0.82	2.23	6.19	2.28	-0.54	1.63	New York, NY-NJ-PA; Los Angeles, CA; Chicago, IL-IN-WI; Dallas, TX; Houston, TX
Sprawling	5.89	5.33	3.32	1.07	2.99	-0.23	-1.12	-0.37	1.31	Glenwood Springs, CO; Gillette, WY; Elko, NV; Show Low, AZ; Jackson, WY-ID
Monocentric	-0.37	-0.55	-0.63	0.76	-0.59	-0.20	-0.33	0.34	53.81	El Paso, TX; Colorado Springs, CO; McAllen, TX; Reno, NV; Lexington, KY
Sprawling-polycentric	1.00	1.33	1.64	0.91	1.78	0.24	0.41	-0.82	8.28	St. Louis, MO-IL; San Diego, CA; Riverside, CA; Tampa, FL; Baltimore, MD
Mixed	0.11	0.26	0.33	0.88	0.27	-0.03	0.35	-0.28	34.97	Denver, CO; Portland, OR-WA; Las Vegas, NV; Orlando, FL; San Antonio, TX

Note: 1) Cells are shaded based on values with darker blue representing greater values. 2) C_{ex} and C_u, though not directly incorporated into the clustering procedure, are also examined to capture the commuting efficiency patterns of each category.

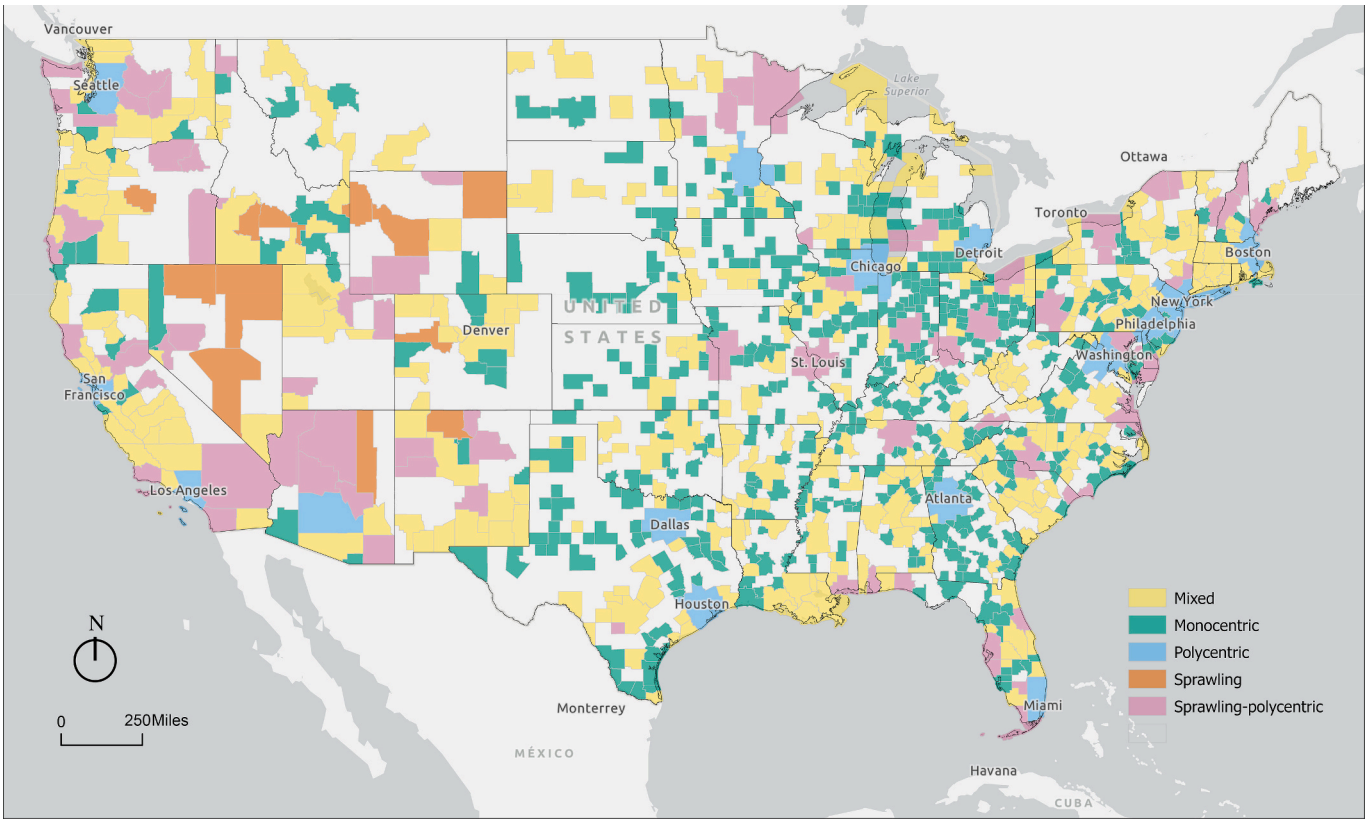

Fig. 5. Spatial distribution of the five MSA categories across the United States.

However, these MSAs show the largest C_u, reflecting their limited commuting capacity due to concentrated jobs-housing distributions.

Sprawling-polycentric. This category, situated between the sprawling and polycentric groups on the SOM map, contains 76 MSAs, such as St. Louis, MO-IL; San Diego, CA; Riverside, CA; Tampa, FL; and Baltimore, MD. It combines features of both sprawling and polycentric development, as reflected by substantial overlaps in the urban triangles. This group shows higher *DI* and slightly increased C_{CBD} and C_{max} values, indicating a general shift toward decentralization and sprawl. Although it has a larger average population, it exhibits lower density and poorer jobs-housing proximity than the polycentric group, as demonstrated by the second largest C_{min}.

Mixed. This category represents the second most prevalent urban form in the United States, encompassing approximately 35 % of MSAs, including Denver, CO; Portland, OR-WA; Las Vegas, NV; Orlando, FL; and San Antonio, TX. Unlike other categories where development is driven by a single dominant pattern, MSAs in this category exhibit a diverse mix of characteristics.

4.3. Environmental and health impacts at commuting extremes across U. S. MSAs

Table 5 presents the total changes in vehicle miles traveled (VMT) and the corresponding vehicle emissions at the two commuting extremes across different urban forms. Across MSAs, the minimum commuting scenario is projected to reduce average one-way trip distances by 6.27 miles per capita, while the maximum commuting scenario anticipates an increase of 16.86 miles per capita for one-way trips. These changes in VMT can significantly impact the environment, particularly reflected in carbon dioxide (CO_2) emissions, which are expected to rise by 670,088 ktons in the maximum scenario and decrease by 249,196 ktons in the minimum scenario, along with changes in Exhaust carbon monoxide (CO) emissions. Fig. 6a illustrates substantial geographic disparities in total VMT and emission changes across MSAs under the two commuting extremes. Overall, given the clear correlation between population size and total VMT, polycentric MSAs—home to the most densely populated metropolitan areas in the United States—are expected to experience the

Table 5
Estimated changes in vehicle emissions under minimum and maximum commuting scenarios across various urban forms.

	Potential emission increase under the maximum commuting scenario					
	Percent (%)	Total HC (ktons)	Exhaust CO (ktons)	NO_x (ktons)	Primary $PM_{2.5}$ (ktons)	CO_2 (ktons)
Polycentric	59.7	351.0	4970.0	274.0	9.6	400,000.0
Sprawling	0.1	0.7	9.8	0.5	0.0	788.0
Monocentric	3.0	17.8	252.0	13.9	0.5	20,300.0
Sprawling-polycentric	17.8	105.0	1490.0	81.9	2.9	120,000.0
Mixed	19.3	113.0	1610.0	88.5	3.1	129,000.0
	Potential emission reduction under the minimum commuting scenario					
Polycentric	55.4	121.0	1710.0	94.4	3.3	138,000.0
Sprawling	0.1	0.2	2.4	0.1	0.0	196.0
Monocentric	4.3	9.3	132.0	7.3	0.3	10,600.0
Sprawling-polycentric	17.2	37.5	531.0	29.3	1.0	42,800.0
Mixed	23.1	50.5	716.0	39.4	1.4	57,600.0

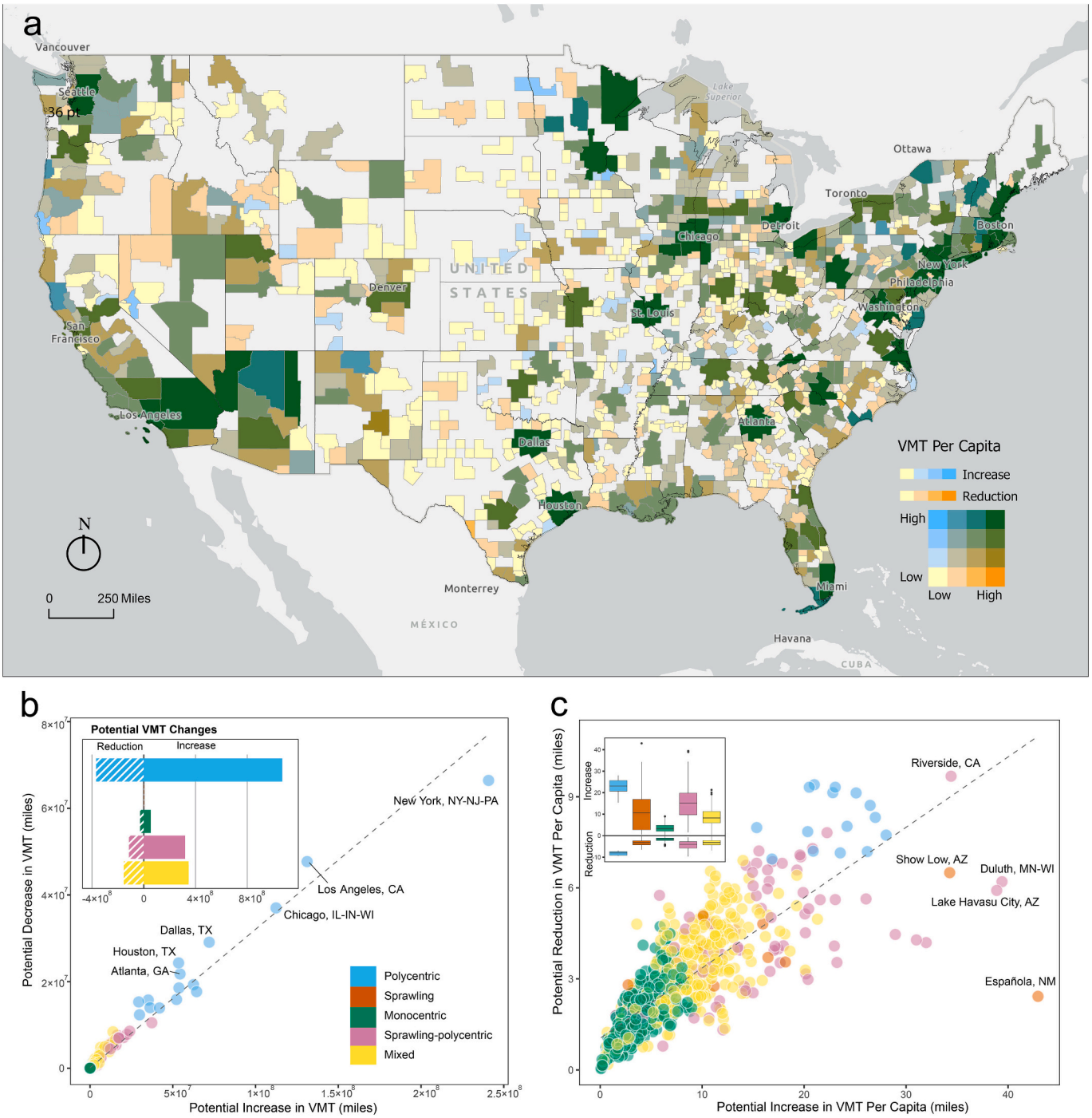

Fig. 6. a, Spatial distribution of changes in VMT per capita; b, distribution of potential changes in VMT across MSAs by urban form; and c, distribution of potential changes in VMT per capita across MSAs by urban form.

most significant shifts. These regions are projected to contribute approximately 60 % of the total increase and 50 % of the reduction in VMT. Notably, about 27 % of the anticipated increase and 22 % of the decrease in VMT are concentrated in the top three metropolitan areas: New York, Los Angeles, and Chicago. Following closely, mixed and sprawling-polycentric MSAs rank as the second and third largest contributors, together accounting for around 30 % to 40 % of the total changes, with monocentric and sprawling MSAs contributing less.

To isolate the effect of population size, changes in VMT per capita are analyzed across MSAs (see Fig. 6). Fig. 6c highlights Riverside as a standout among the MSAs, indicating the highest potential change in VMT per capita. Additionally, polycentric MSAs such as New York, Philadelphia, Washington DC, Detroit, Chicago, Seattle, Los Angeles, Dallas, and Houston exhibit more significant changes in VMT per capita under both extreme commuting scenarios, owing to the broader commuting range enabled by their urban form. Conversely, some sprawling and sprawling-polycentric MSAs, like Española, NM and Lake Havasu City, AZ display greater potential increases in VMT per capita under the maximum commuting scenario, yet they show limited potential for savings due to their relatively imbalanced jobs-housing distribution.

Table 6 presents the total changes in mortality associated with various emissions sources ($PM_{2.5}$, VOC, NOX) as estimated by the three reduced-complexity air quality health effect models (see the Methods

section for more details). Overall, the findings indicate a high level of consistency among the models, with discrepancies between the highest and lowest estimates remaining under 14 %. The average mortality change across the three models shows that NOX is the primary contributor to mortality changes, accounting for over 51.1 % of the reduction and 51.2 % of the increase on average, followed by $PM_{2.5}$ and VOC.

In general, reducing EC can yield substantial health benefits. The minimum commuting scenario has the potential to prevent 1273 deaths. Conversely, if the commuting distances in the 918 MSAs continue to expand to the maximum scenario, there is an estimated increase of 3480 deaths due to elevated vehicle emissions. Fig. 7b presents a detailed examination of the potential mortality changes across MSAs with distinct urban forms under the two extreme commuting scenarios. A polarized pattern emerges in health outcomes across MSAs, reflecting a similar trend observed in environmental impacts. The densely populated polycentric MSAs are projected to undergo the most significant potential health impacts, making up approximately 72 % of reductions and 76 % of increases in mortality. This trend is followed by the sprawling-polycentric and mixed MSAs. In particular, the top three metropolitan areas—New York, Los Angeles, and Chicago—demonstrate potential reductions (increases) in deaths of 266 (884), 177 (490), and 110 (313) respectively. These figures represent nearly 45 % (48 %) of the total mortality changes under the two extreme commuting scenarios.

Examining the average mortality changes scaled by population size reveals a distinct pattern (see Fig. 7a and 7c). Generally, mortality savings and increases exhibit a clear linear relationship. Geographically, the northeastern and Great Lakes regions, as well as Dallas and its surrounding MSAs, exhibit higher mortality changes. Notably, there are large disparities across different urban form categories and even within the same category. Among polycentric MSAs, New York, Los Angeles, and Chicago demonstrate higher mortality changes per 1000 people under the two extreme commuting scenarios compared to other MSAs. Philadelphia and Detroit also stand out, due to disproportional mortality increase and saving, respectively. Interestingly, despite experiencing greater changes in VMT and vehicle emissions, the health outcomes for certain large polycentric MSAs like Seattle, WA; Miami, FL; and Phoenix, AZ seem to be less pronounced under the two extreme commuting scenarios due to factors such as frequent rainfall, strong wind patterns, and unique geographical features that help disperse pollutants. Smaller MSAs also warrant closer attention. For example, several monocentric MSAs, such as Bonham, TX; Jefferson, GA; Urbana, OH; and Bennettsville, SC stand out due to higher mortality changes.

5. Conclusions

This study examines changes in air pollutant levels and resulting mortality as commutes within MSAs across the United States approach their two extremes: the shortest (minimum) and longest (maximum) commutes possible based on each MSA's existing urban form. The results highlight a significant reduction in vehicle emissions when commuting distances are minimized to their lower extreme, with an average reduction of 6.27 miles per capita. This shift leads to substantial decreases in total HC, exhaust CO, NO_x, primary $PM_{2.5}$, and CO_2 emissions. Conversely, if commuting distances extend toward the upper extreme without policy intervention, an increase of 16.86 miles per capita could significantly worsen air pollution. Environmental impacts differ significantly across MSAs, with total changes in VMT and vehicle emissions closely tied to population size. Densely populated polycentric MSAs—particularly New York, Los Angeles, and Chicago—are key contributors to overall changes in VMT and air pollution in the nation under both extreme commuting scenarios. However, per capita VMT changes highlight MSAs with greater commuting capacity, such as Riverside, along with sprawling MSAs that exhibit higher upper commuting limits.

The health impacts are substantial, emphasizing the urgency for policy interventions to reduce commuting burdens in urban areas. By cutting commuting-related vehicle emissions across MSAs, an estimated 1273 deaths could be prevented under the minimum commuting scenario. Conversely, the maximum commuting scenario could lead to an additional 3480 deaths. Health outcomes vary significantly across different urban forms. Around 72 % of the total mortality reductions and 76 % of the increases are concentrated in polycentric MSAs, particularly in New York, Los Angeles, and Chicago. As major contributors to these mortality changes, these densely populated regions require targeted sustainable urban planning policies. Importantly, in polycentric regions with relatively balanced jobs-housing distributions, land-use policies that simply promote jobs-housing balance may fall short. A more thorough investigation into the factors driving EC is needed. For example, policies targeting jobs-housing fit (Blumenberg and Siddiq, 2023), like affordable housing initiatives, are essential for addressing commuting inefficiencies and associated environmental and health impacts effectively. The pattern of mortality changes per 1000 people reveals interesting geographic trends. Notably, health outcomes don't always align directly with emission changes. For example, despite notable environmental impacts, large polycentric MSAs like Seattle, WA; Miami, FL; and Phoenix, AZ show relatively lower health impacts due to geographic factors that help disperse pollutants. In contrast, smaller monocentric MSAs such as Bonham, TX; Jefferson, GA; Urbana, OH; and Bennettsville, SC exhibit significant health impacts under both extreme commuting scenarios.

The study has several limitations. First, the LEHD dataset does not differentiate between transportation modes, so it is assumed that all commuters drive alone to work. This assumption could affect the accuracy of EC and vehicle emissions estimates, particularly in cities with higher public transit use. Second, the analysis does not explicitly incorporate the growing prevalence of remote and hybrid work arrangements, especially in the post-COVID-19 era. These evolving work patterns may substantially reshape commuting patterns by reducing overall travel demand, altering the spatial interactions between jobs and housing locations, and creating new temporal rhythms of mobility. Future research could extend this framework to capture partial or flexible commuting schedules, as well as the experiences of individuals with multiple or rotating worksites, which add further complexity to the commuting landscape. Third, this study assumes a uniform per-mile emission rate for each pollutant, without differentiating by vehicle age, make, or model. Because per-mile emission rates continue to decline with technological improvements and stricter standards, future air pollution and related health impacts may become less sensitive to commuting distance alone. Moreover, the growing adoption of electric vehicles (EVs) introduces new spatial and environmental dynamics: while EVs reduce tailpipe emissions, they shift the emission source to electricity generation, the intensity of which varies geographically with regional energy mixes. Considering these ongoing transformations in work practices and vehicle technologies is crucial for interpreting the

Table 6
Estimated mortality changes (number of deaths) from air pollutants under minimum and maximum commuting scenarios.

Potential mortality reduction under the minimum commuting scenario				
Model	From Primary $PM_{2.5}$	From VOC	From NO_X	Total
EASIUR	372	277	669	1318
AP3	392	277	603	1272
InMAP	334	216	678	1228

Potential mortality increase under the maximum commuting scenario				
Model	From Primary $PM_{2.5}$	From VOC	From NO_X	Total
EASIUR	1045	760	1962	3767
AP3	1069	760	1608	3437
InMAP	897	568	1772	3237

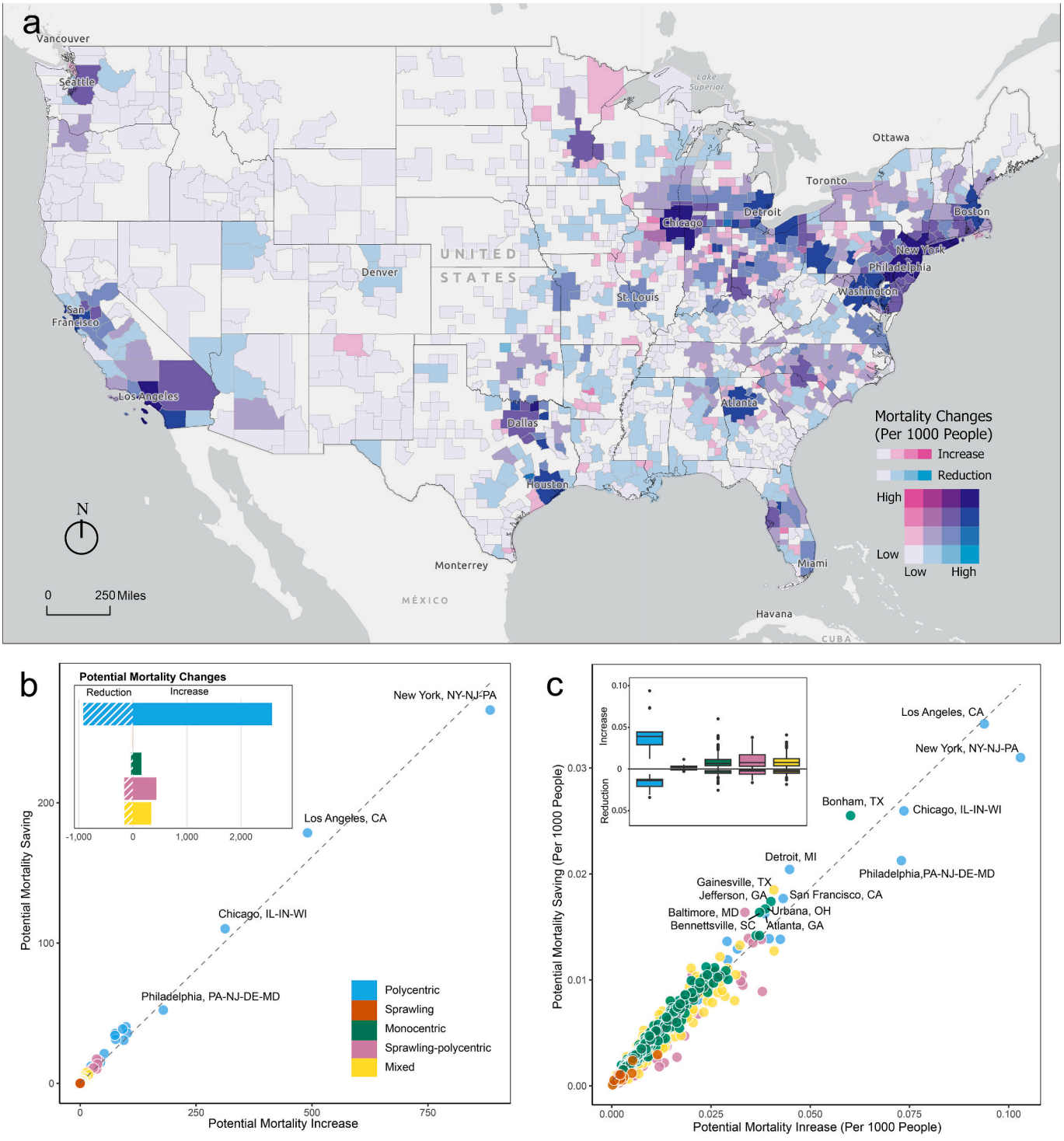

Fig. 7. a, Spatial variation of mortality changes per 1000 people; b, distribution of potential changes in mortality across MSAs by urban form; and c, distribution of potential changes in mortality changes per 1000 people across MSAs by urban form.

long-term implications of commuting efficiency, air quality, and public health. Fourth, while the study utilizes three reduced-complexity air quality models to provide a comprehensive assessment of potential health benefits from optimal commuting, the benefits of ozone (O_3) reduction are underrepresented, as these models primarily focus on $PM_{2.5}$-related health impacts. Finally, to enhance accuracy and reliability, the health findings should be further validated using a full-scale chemical transport model in conjunction with the health impacts model.

CRediT authorship contribution statement

Yue Jing: Writing – original draft, Visualization, Methodology, Formal analysis, Data curation. **Yujie Hu:** Writing – review & editing, Supervision, Resources, Methodology, Conceptualization. **Chen Chen:** Writing – original draft, Validation, Methodology, Formal analysis. **Daniel S. Cohan:** Writing – review & editing, Resources, Methodology, Conceptualization.

Data availability

Data will be made available on request.

References

Aguiléra, A., Voisin, M., 2014. Urban form, commuting patterns and CO2 emissions: what differences between the municipality's residents and its jobs? Transp. Res. A Policy Pract. 69, 243–251.

Arribas-Bel, D., Schmidt, C.R., 2013. Self-organizing maps and the US urban spatial structure. Environ. Plann. B. Plann. Des. 40 (2), 362–371. https://doi.org/10.1068/b37014.

Baltimore City Department of Housing & Community Development, 2021. Live Near Your Work. Retrieved October 30, 2025, from. https://livebaltimore.com/resident-resources/financial-incentives/live-near-your-work/.

Bereitschaft, B., Debbage, K., 2013. Urban form, air pollution, and CO2 emissions in large US metropolitan areas. Prof. Geogr. 65 (4), 612–635.

Blaudin de Thé, C., Carantino, B., Lafourcade, M., 2021. The carbon 'carprint' of urbanization: new evidence from French cities. Reg. Sci. Urban Econ. 89, 103693. https://doi.org/10.1016/j.regsciurbeco.2021.103693.

Blumenberg, E., Siddiq, F., 2023. Commute distance and jobs-housing fit. Transportation 50 (3), 869–891. https://doi.org/10.1007/s11116-022-10264-1.

Boarnet, M.G., 2011. A broader context for land use and travel behavior, and a research agenda. J. Am. Plan. Assoc. 77 (3), 197–213. https://doi.org/10.1080/01944363.2011.593483.

Boarnet, M., Crane, R., 2001. The influence of land use on travel behavior: specification and estimation strategies. Transp. Res. A Policy Pract. 35 (9), 823–845. https://doi.org/10.1016/S0965-8564(00)00019-7.

Brotchie, J.F., 1984. Technological change and urban form. Environ. Plan. A Econ. Space 16 (5), 583–596. https://doi.org/10.1068/a160583.

Bruns, A., Matthes, G., 2019. Moving into and within cities – interactions of residential change and the travel behavior and implications for integrated land use and transport planning strategies. Travel Behav. Soc. 17, 46–61. https://doi.org/10.1016/j.tbs.2019.06.002.

Buliung, R.N., Kanaroglou, P.S., 2002. Commute minimization in the Greater Toronto Area: applying a modified excess commute. J. Transp. Geogr. 10 (3), 177–186. https://doi.org/10.1016/S0966-6923(02)00010-8.

Burgalassi, D., Luzzati, T., 2015. Urban spatial structure and environmental emissions: a survey of the literature and some empirical evidence for Italian NUTS 3 regions. Cities 49, 134–148. https://doi.org/10.1016/j.cities.2015.07.008.

Byun, D., Schere, K.L., 2006. Review of the governing equations, computational algorithms, and other components of the models-3 community multiscale air quality (CMAQ) modeling system. Appl. Mech. Rev. 59 (2), 51–77. https://doi.org/10.1115/1.2128636.

Cervero, R., 1989. Jobs-housing balancing and regional mobility. J. Am. Plan. Assoc. 55 (2), 136–150. https://doi.org/10.1080/01944368908976014.

Charron, M., 2007. From excess commuting to commuting possibilities: more extension to the concept of excess commuting. Environ. Plan. A Econ. Space 39 (5), 1238–1254. https://doi.org/10.1068/a3897.

Chen, C., McCabe, D.C., Fleischman, L.E., Cohan, D.S., 2022. Black carbon emissions and associated health impacts of gas flaring in the United States. Atmosphere 13 (3). https://doi.org/10.3390/atmos13030385. Article 3.

Chowdhury, T.A., Scott, D.M., Kanaroglou, P.S., 2013. Urban form and commuting efficiency: a comparative analysis across time and space. Urban Stud. 50 (1), 191–207. https://doi.org/10.1177/0042098012452324.

Delmelle, E.C., 2017. Differentiating pathways of neighborhood change in 50 U.S. metropolitan areas. Environ. Plan. A Econ. Space 49 (10), 2402–2424. https://doi.org/10.1177/0308518X17722564.

District of Columbia Office of Planning, 2011. Live Near Your Work. Retrieved October 30, 2025, from. https://planning.dc.gov/page/live-near-your-work.

ENVIRON, 2014. User's Guide to the Comprehensive Air Quality Model with Extensions (CAMx). https://www.camx.com.

Frost, M., Linneker, B., Spence, N., 1998. Excess or wasteful commuting in a selection of British cities. Transp. Res. A Policy Pract. 32 (7), 529–538. https://doi.org/10.1016/S0965-8564(98)00016-0.

Gilmore, E.A., Heo, J., Muller, N.Z., Tessum, C.W., Hill, J.D., Marshall, J.D., Adams, P.J., 2019. An inter-comparison of the social costs of air quality from reduced-complexity models. Environ. Res. Lett. 14 (7), 074016. https://doi.org/10.1088/1748-9326/ab1ab5.

Grell, G.A., Peckham, S.E., Schmitz, R., McKeen, S.A., Frost, G., Skamarock, W.C., Eder, B., 2005. Fully coupled "online" chemistry within the WRF model. Atmos. Environ. 39 (37), 6957–6975. https://doi.org/10.1016/j.atmosenv.2005.04.027.

Ha, J., Lee, S., Kwon, S.M., 2021. Revisiting the relationship between urban form and excess commuting in US metropolitan areas. J. Plan. Educ. Res. 41 (3), 294–311. https://doi.org/10.1177/0739456X18787886.

Hamilton, B.W., Röell, A., 1982. Wasteful commuting. J. Polit. Econ. 90 (5), 1035–1053. https://doi.org/10.1086/261107.

Health Effects Institute, 2024. State of Global Air 2024 [Special Report]. Health Effects Institute.

Heo, J., Adams, P.J., Gao, H.O., 2016. Public health costs of primary PM2.5 and inorganic PM2.5 precursor emissions in the United States. Environ. Sci. Technol. 50 (11), 6061–6070. https://doi.org/10.1021/acs.est.5b06125.

Horner, M.W., 2002. Extensions to the concept of excess commuting. Environ. Plan. A Econ. Space 34 (3), 543–566. https://doi.org/10.1068/a34126.

Horner, M.W., Schleith, D., 2012. Analyzing temporal changes in land-use–transportation relationships: a LEHD-based approach. Appl. Geogr. 35 (1), 491–498. https://doi.org/10.1016/j.apgeog.2012.09.006.

Hu, Y., Li, X., 2021. Modeling and analysis of excess commuting with trip chains. Ann. Am. Assoc. Geogr. 111 (6), 1851–1867. https://doi.org/10.1080/24694452.2020.1835461.

Hu, Y., Wang, F., 2016. Temporal trends of intraurban commuting in Baton Rouge, 1990–2010. Ann. Am. Assoc. Geogr. 106 (2), 470–479. https://doi.org/10.1080/00045608.2015.1113117.

Hu, Y., Wang, C., Li, R., Wang, F., 2020. Estimating a large drive time matrix between ZIP codes in the United States: a differential sampling approach. J. Transp. Geogr. 86, 102770. https://doi.org/10.1016/j.jtrangeo.2020.102770.

Industrial Economics, Inc, 2019. Evaluating Reduced-form Tools for Estimating Air Quality Benefits. https://www.epa.gov/sites/default/files/2020-09/documents/iec_rft_report_9.15.19.pdf.

Jing, Y., Hu, Y., 2024. Multiscale complex network analysis of commuting efficiency: urban connectivity, hierarchy, and labor market. Ann. Am. Assoc. Geogr. 114 (8), 1681–1692. https://doi.org/10.1080/24694452.2023.2284296.

Jing, Y., Hu, Y., Niedzielski, M.A., 2023. Neighborhood divides: where you live matters for commuting and its efficiency. Cities 132, 104091. https://doi.org/10.1016/j.cities.2022.104091.

Kanaroglou, P.S., Higgins, C.D., Chowdhury, T.A., 2015. Excess commuting: a critical review and comparative analysis of concepts, indices, and policy implications. J. Transp. Geogr. 44, 13–23. https://doi.org/10.1016/j.jtrangeo.2015.02.009.

Kim, K., Horner, M.W., 2021. Examining the impacts of the great recession on the commuting dynamics and jobs-housing balance of public and private sector workers. J. Transp. Geogr. 90, 102933. https://doi.org/10.1016/j.jtrangeo.2020.102933.

Korsu, E., Le Néchet, F., 2017. Would fewer people drive to work in a city without excess commuting? Explorations in the Paris metropolitan area. Transp. Res. A Policy Pract. 95, 259–274. https://doi.org/10.1016/j.tra.2016.10.030.

Krewski, D., Jerrett, M., Burnett, R.T., Ma, R., Hughes, E., Shi, Y., Turner, M.C., Pope, C. A., Thurston, G., Calle, E.E., Thun, M.J., Beckerman, B., DeLuca, P., Finkelstein, N., Ito, K., Moore, D.K., Newbold, K.B., Ramsay, T., Ross, Z., Tempalski, B., 2009. Extended follow-up and spatial analysis of the American Cancer Society study linking particulate air pollution and mortality. Res. Rep. Health Eff. Inst. 140, 5–114 discussion 115-136.

Lee, C., 2020. Metropolitan sprawl measurement and its impacts on commuting trips and road emissions. Transp. Res. Part D: Transp. Environ. 82, 102329.

Lepeule, J., Laden, F., Dockery, D., Schwartz, J., 2012. Chronic exposure to fine particles and mortality: an extended follow-up of the Harvard six cities study from 1974 to 2009. Environ. Health Perspect. 120 (7), 965–970. https://doi.org/10.1289/ehp.1104660.

Loo, B.P.Y., Chow, A.S.Y., 2011. Jobs-housing balance in an era of population decentralization: an analytical framework and a case study. J. Transp. Geogr. 19 (4), 552–562. https://doi.org/10.1016/j.jtrangeo.2010.06.004.

Ma, K.-R., Banister, D., 2006. Extended excess commuting: a measure of the jobs-housing imbalance in Seoul. Urban Stud. 43 (11), 2099–2113. https://doi.org/10.1080/00420980600945245.

Ma, K.R., Banister, D., 2007. Urban spatial change and excess commuting. Environ. Plan. A 39 (3), 630–646.

Muller, N.Z., 2014. Boosting GDP growth by accounting for the environment. Science 345 (6199), 873–874. https://doi.org/10.1126/science.1253506.

Muñiz, I., Garcia-López, M.-À., 2019. Urban form and spatial structure as determinants of the ecological footprint of commuting. Transp. Res. Part D: Transp. Environ. 67, 334–350. https://doi.org/10.1016/j.trd.2018.08.006.

Muñiz, I., Rojas, C., 2019. Urban form and spatial structure as determinants of per capita greenhouse gas emissions considering possible endogeneity and compensation behaviors. Environ. Impact Assess. Rev. 76, 79–87.

Murphy, E., Killen, J.E., 2011. Commuting economy: an alternative approach for assessing regional commuting efficiency. Urban Stud. 48 (6), 1255–1272. https://doi.org/10.1177/0042098010370627.

Sacks, J.D., Lloyd, J.M., Zhu, Y., Anderton, J., Jang, C.J., Hubbell, B., Fann, N., 2018. The environmental benefits mapping and analysis program - community edition (BenMAP-CE): a tool to estimate the health and economic benefits of reducing air pollution. Environ. Model Softw. 104, 118–129.

Schleith, D., Widener, M.J., Kim, C., Horner, M.W., 2019. Categorizing urban form for the largest metro regions in the U.S. using the excessive commuting framework. Built Environ. 45 (4), 450–461. https://doi.org/10.2148/benv.45.4.450.

Schwanen, T., Dieleman, F.M., Dijst, M., 2004. The impact of metropolitan structure on commute behavior in the Netherlands: a multilevel approach. Growth Chang. 35 (3), 304–333. https://doi.org/10.1111/j.1468-2257.2004.00251.x.

Scott, D.M., Kanaroglou, P.S., Anderson, W.P., 1997. Impacts of commuting efficiency on congestion and emissions: case of the Hamilton CMA, Canada. Transp. Res. Part D: Transp. Environ. 2 (4), 245–257. https://doi.org/10.1016/S1361-9209(97)00015-1.

Skamarock, W., Klemp, J., Dudhia, J., Gill, D., Barker, D., Wang, W., Huang, X.-Y., Duda, M., 2008. A Description of the Advanced Research WRF Version 3. UCAR/NCAR. http://opensky.ucar.edu/islandora/object/technotes:500.

Sultana, S., 2002. Job/housing imbalance and commuting time in the Atlanta metropolitan area: exploration of causes of longer commuting time. Urban Geogr. 23 (8), 728–749. https://doi.org/10.2747/0272-3638.23.8.728.

Susilo, Y.O., Maat, K., 2007. The influence of built environment to the trends in commuting journeys in the Netherlands. Transportation 34 (5), 589–609. https://doi.org/10.1007/s11116-007-9129-5.

Tapestry Segmentation—Esri Demographics Regional Data | Documentation, 2020 [Dataset]. Retrieved September 30, 2024, from. https://doc.arcgis.com/en/esri-demographics/latest/regional-data/tapestry-segmentation.html.

Tessum, C.W., Hill, J.D., Marshall, J.D., 2017. InMAP: a model for air pollution interventions. PLoS One 12 (4), e0176131. https://doi.org/10.1371/journal.pone.0176131.

Turner, D.B., 2020. Workbook of Atmospheric Dispersion Estimates: An Introduction to Dispersion Modeling, Second Edition, 2nd ed. CRC Press.

U.S. Environmental Protection Agency, 2020. Smog, Soot, and Other Air Pollution from Transportation [Overviews and Factsheets]. https://www.epa.gov/transportation-air-pollution-and-climate-change/smog-soot-and-other-air-pollution-transportation.

Welch, T.F., Mishra, S., 2014. Envisioning an emission diet: application of travel demand mechanisms to facilitate policy decision making. Transportation 41 (3), 611–631. https://doi.org/10.1007/s11116-013-9511-4.

White, M.J., 1988. Urban commuting journeys are not "wasteful". Journal of Political Economy 96 (5), 1097–1110.

Woodruff, T.J., Parker, J.D., Schoendorf, K.C., 2006. Fine particulate matter (PM2.5) air pollution and selected causes of postneonatal infant mortality in California. Environ. Health Perspect. 114 (5), 786–790. https://doi.org/10.1289/ehp.8484.

Xu, W., Yang, L., Zhang, W., 2019. Evaluation of transport policy packages in the excess commuting framework: the case of Xiamen, China. Cities 87, 39–47. https://doi.org/10.1016/j.cities.2018.12.009.

Yang, J., 2008. Policy implications of excess commuting: examining the impacts of changes in US metropolitan spatial structure. Urban Stud. 45 (2), 391–405. https://doi.org/10.1177/0042098007085969.

Yue, L., Niedzielski, M.A., O'Kelly, M.E., 2024. Modal disparity in commuting efficiency: a comparison across educational worker subgroups in Shanghai. Cities 147, 104790. https://doi.org/10.1016/j.cities.2024.104790.

Zhang, B., Xin, Q., Chen, S., Yang, Z., Wang, Z., 2024. Urban spatial structure and commuting-related carbon emissions in China: do monocentric cities emit more? Energy Policy 186, 113990. https://doi.org/10.1016/j.enpol.2024.113990.

Zhou, J., Murphy, E., Corcoran, J., 2020. Integrating road carrying capacity and traffic congestion into the excess commuting framework: the case of Los Angeles. Environ. Plan. B Urban Anal. City Sci. 47 (1), 119–137. https://doi.org/10.1177/2399808318773762.